

## Versatile synthesis for PBCA-based hybrid fluorescent microbubbles and their potential theranostic applications to cell labelling and imaging

Zhe Liu,<sup>a\*</sup> Patrick Koczera,<sup>a</sup> Dennis Doleschel,<sup>a</sup> Fabian Kiessling<sup>a</sup> and Jessica Gätjens<sup>a</sup>

<sup>a</sup> Department of Experimental Molecular Imaging (ExMI), Helmholtz Institute, Medical Faculty, RWTH Aachen University, Aachen 52074, Germany

### Supplementary Information

i) Synthetic protocols for PBCA-based hybrid microbubbles.

One-pot synthesis:<sup>1,2</sup> Ultrasmall superparamagnetic iron oxide (USPIO) nanoparticles were prepared by a co-precipitation method of ferrous and ferric salts according to Khalafalla-Reimers procedure.<sup>3</sup> The hybrid microbubbles were fabricated following a slightly modified protocol as previously published.<sup>4</sup> Deionized water (300 mL) and Triton X-100 (3 mL, 5.0 mmol) were stirred at room temperature in a beaker. The pH was adjusted to 2.5 with HCl (1 M) and 10 mL of the freshly prepared USPIO suspension was added before stirring for 2 min. Butyl cyanoacrylate (BCA, 3 mL, 28.3 mmol) and Rhodamine B dyes (5.0 mg, 0.01 mmol) was added, and then the mixture was stirred by an Ultra Turrax (IKA Werke, Staufen, Germany) (10,000 rpm) at room temperature for 60 min. In this process of polymerization of BCA, hydroxyl anion ( $\text{OH}^-$ ) played the role of activating this reaction as the initiator. In the presence of Triton X-100 as stabilizers and of 2.5 pH medium, the emulsion polymerization can be easily generated by high-speed agitation, which is also a general mechanism for the polymerization of PBCA.<sup>1</sup> Afterwards, the resulting emulsion was then centrifuged (500 rpm, 3×20 min, Heraeus Multifuge, Thermo Scientific, USA) to afford the monodispersed bubble populations. The resulted bubble emulsion was redispersed in 50 ml of Triton X-100 solution (pH 7.0, 0.02%) for storage at 4°C.

Step-wise synthesis: this protocol is slightly different from the above-mentioned one-pot protocol in the fluorescent dyes addition step. After formation of pure PBCA or magnetic microbubbles, the suspension was transferred into a glass vial where aqueous solution of fluorescent dyes was mixed, and magnetic stirring was performed for additional 1h. After this

step, identical centrifugation and size-isolation procedures afforded monodispersed fluorescent bubble populations.

ii) Characterization and imaging.

Proton nuclear magnetic resonance ( $^1\text{H}$  NMR) experiments were performed using a 400 MHz NMR spectrometer (Bruker Biospin GmbH, Germany). Spectra were recorded with characteristic chemical shifts in ppm from TMS with solvent resonance as the internal standard (deuteriochloroform:  $\delta = 7.27$  ppm). Infrared data was acquired by a Perkin-Elmer FT-IR spectrometer (Spectrum 100, Germany) with the expression of absorption peaks in wavenumber ( $\text{cm}^{-1}$ ). The iron concentration and content of fluorescent dyes were determined by inductively coupled plasma mass spectrometer (ICP-MS, Elan-DRCII, Perkin-Elmer, USA) and UPLC-MS (Acquity UPLC, Waters Corp., USA) respectively. Size and volume distribution of various samples were analyzed by using Beckmann Coulter Counter (Multisizer 3 Beckmann Coulter Inc., USA). Surface morphology of PBCA microbubbles was imaged on a scanning electron microscopy (SEM, FEI (PHILIPS) ESEM XL 30 FEG, EDAX Falcon genesis, Netherlands). The morphology of the iron oxide nanoparticles and the embedding structure were characterized using transmission electron microscopy (EM 400T Philips, Netherlands). Optical and fluorescence microscopy (Axio Imager M2, Carl Zeiss Microimaging GmbH, Jena, Germany) was also used to visualize the shape of hybrid fluorescent microbubbles. A multi-photon microscopy system (Olympus FV1000MPE, Japan) was used to acquire the TPLSM images. Subcutaneous injection of non-targeted fluorescent and fluomagnetic microbubbles into nude mice was detected with a FluoVivo 300 fluorescent imaging platform (INDEC Biosystems, USA).

iii) MR imaging with VEGFR2-targeting fluomagnetic microbubbles.

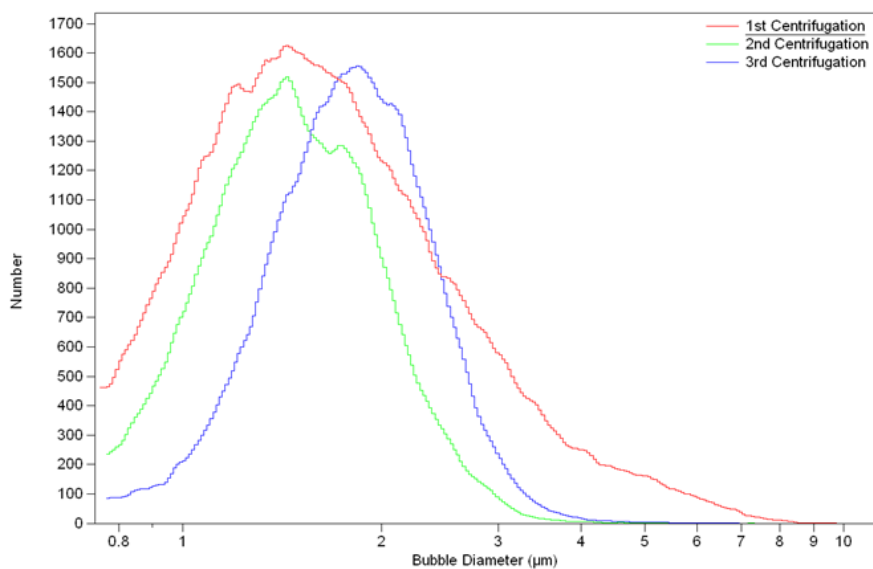
By using a 3.0-T clinical whole-body MRI scanner (Achieva 3.0T Philips, Netherlands) equipped with a mouse coil, in vivo  $T_2^*$ -weighted echo planar imaging (EPI) dynamic contrast-enhanced (DCE) MR imaging with nude mice was performed before and after i.v. bubble administration to monitor the contrast. Twenty seconds after the EPI DCE MR sequence was activated, 100  $\mu\text{L}$  of microbubbles were injected. The sequence parameters were (repetition time (TR) = 71 ms, echo time (TE) = 11 ms, number of excitations (NEX) = 1, slice thickness = 2 mm, field of view (FOV) = 30 mm  $\times$  8 mm, matrix size = 64  $\times$  60,

number of dynamic measurements 600, and total scan time = 533 s. To evaluate the contrast, signal intensities (SI) were measured before and after injection of the magnetic microbubbles. SI over time curves were generated in a defined region of interest (ROI) covering the tumor using the imaging analysis software Dynalab (MEVIS Research, Bremen, Germany). The T<sub>2</sub>-weighted MR images of the tumor before MBs injection were obtained with a TSE sequence (TR = 2391 ms, TE = 100 ms, NEX = 3, slice thickness = 1 mm, FOV = 25 mm × 22 mm, matrix size = 124 × 120).

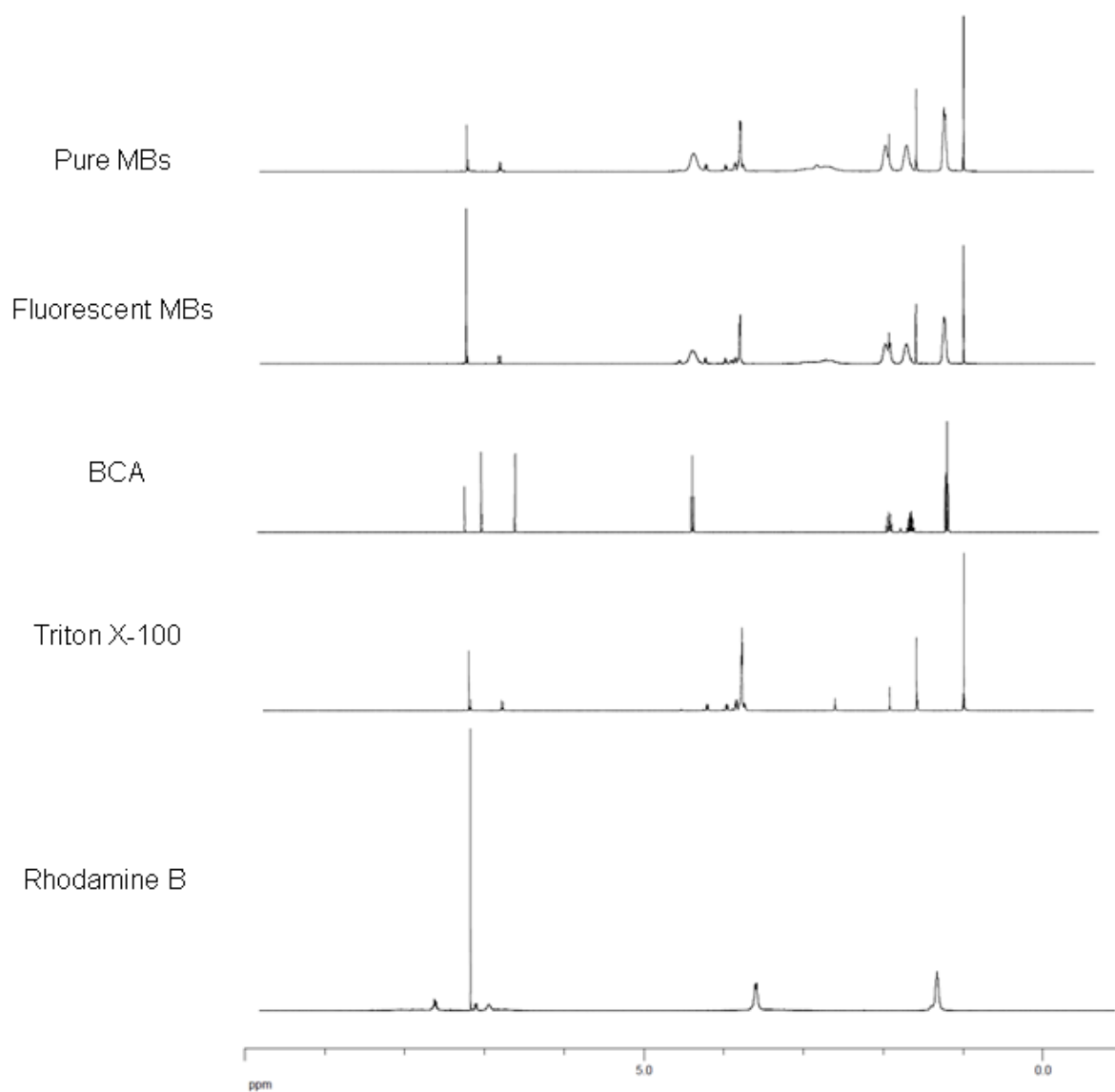
#### References:

1. N. Behan, C. Birkinshaw and N. Clarke, *Biomaterials*, 2001, **22**, 1335.
2. C. Olbrich, P. Hauff, F. Scholle, W. Schmidt, U. Bakowsky, A. Briel et al. *Biomaterials*, 2006, **27**, 3549.
3. S. E. Khalafalla and G. W. Reimers, *IEEE Trans. Magn.*, 1980, **16**, 178.
4. Z. Liu, T. Lammers, J. Ehling, S. Fokong, J. Bornemann, F. Kiessling and J. Gätjens, *Biomaterials*, 2011, **32**, 6155.

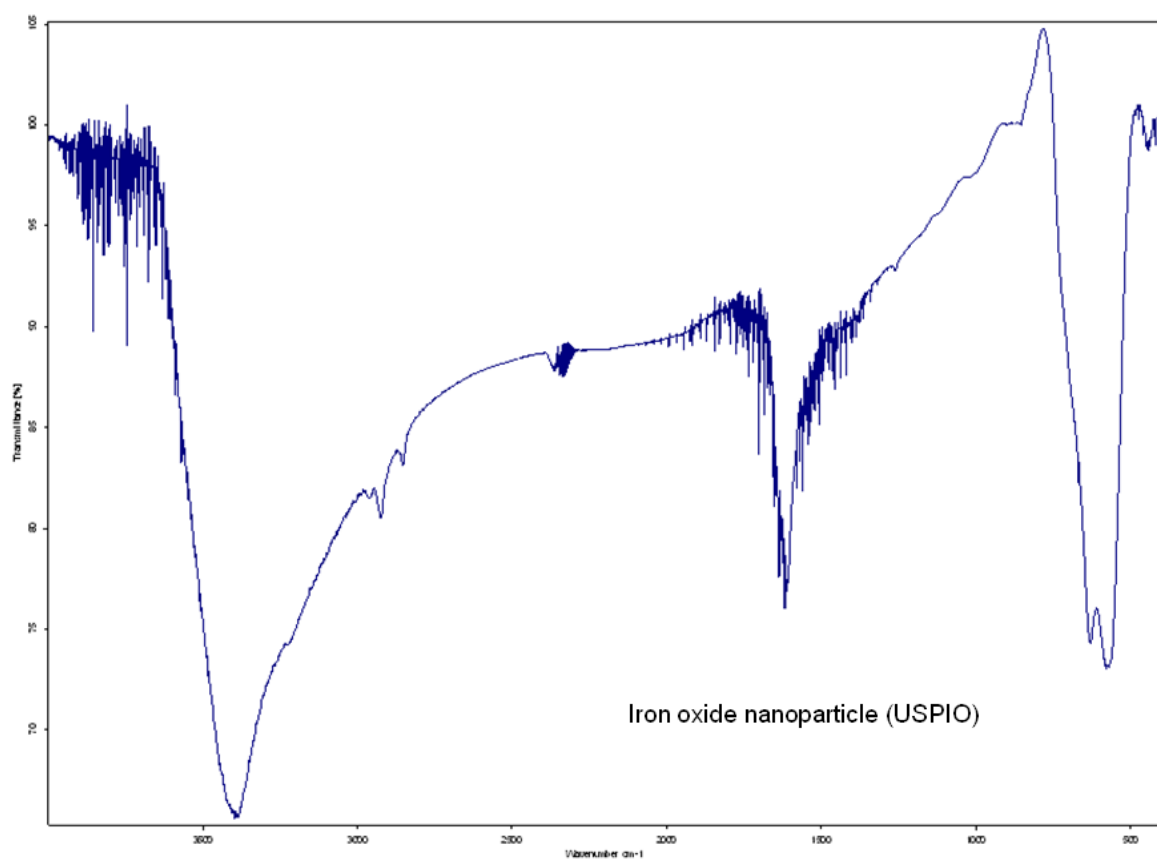
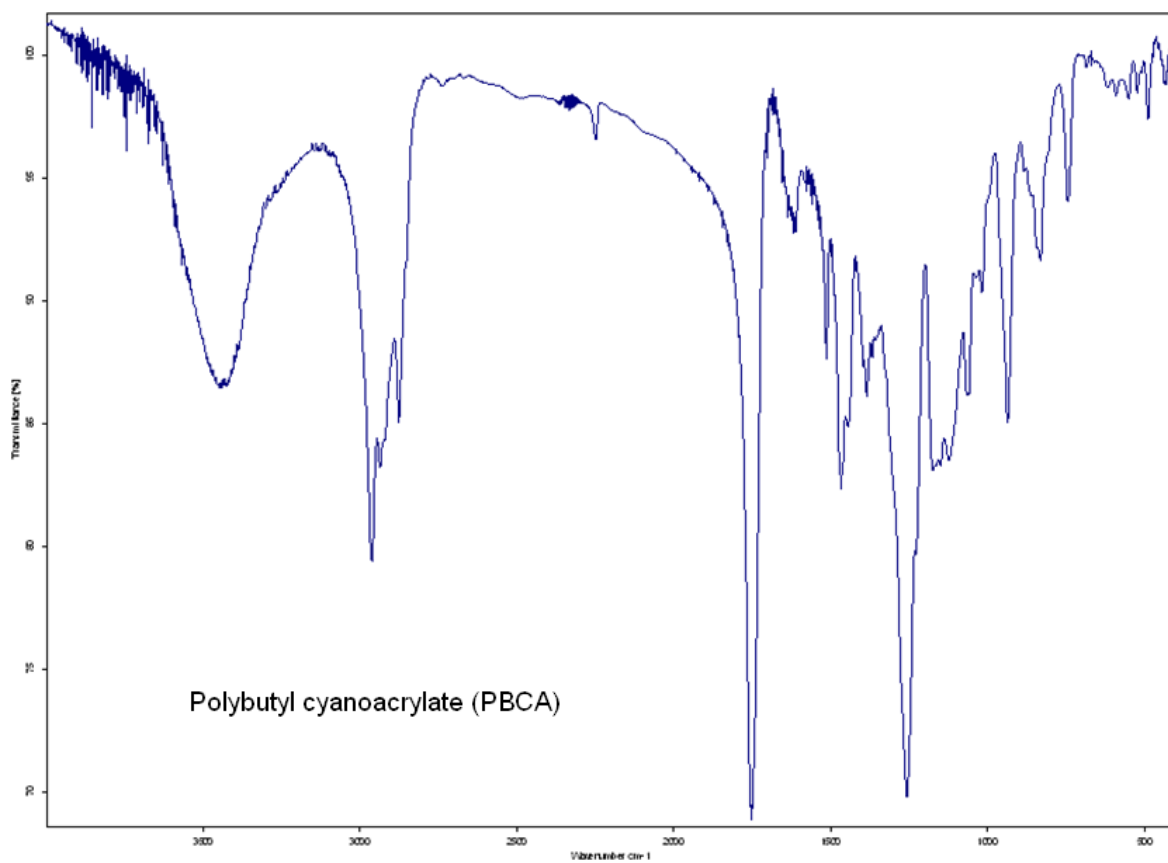
### Supplementary Figures:

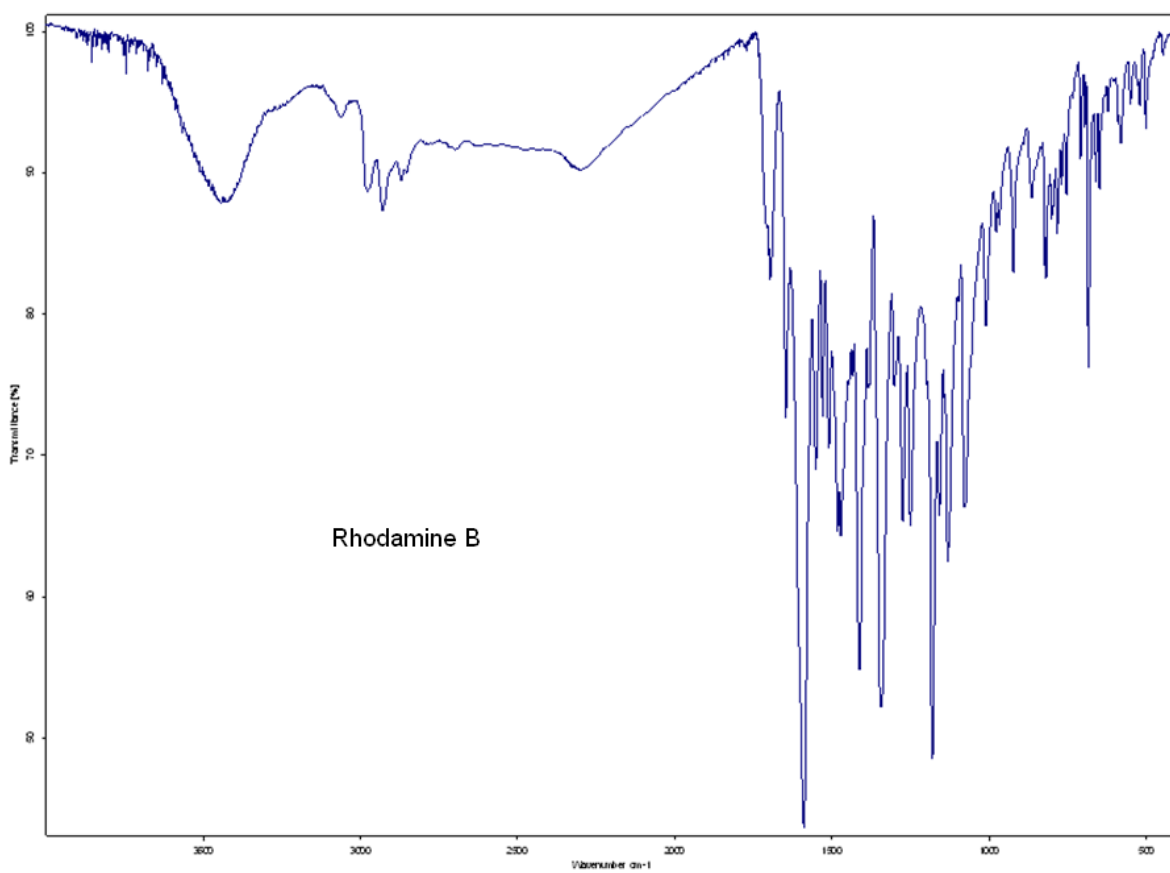
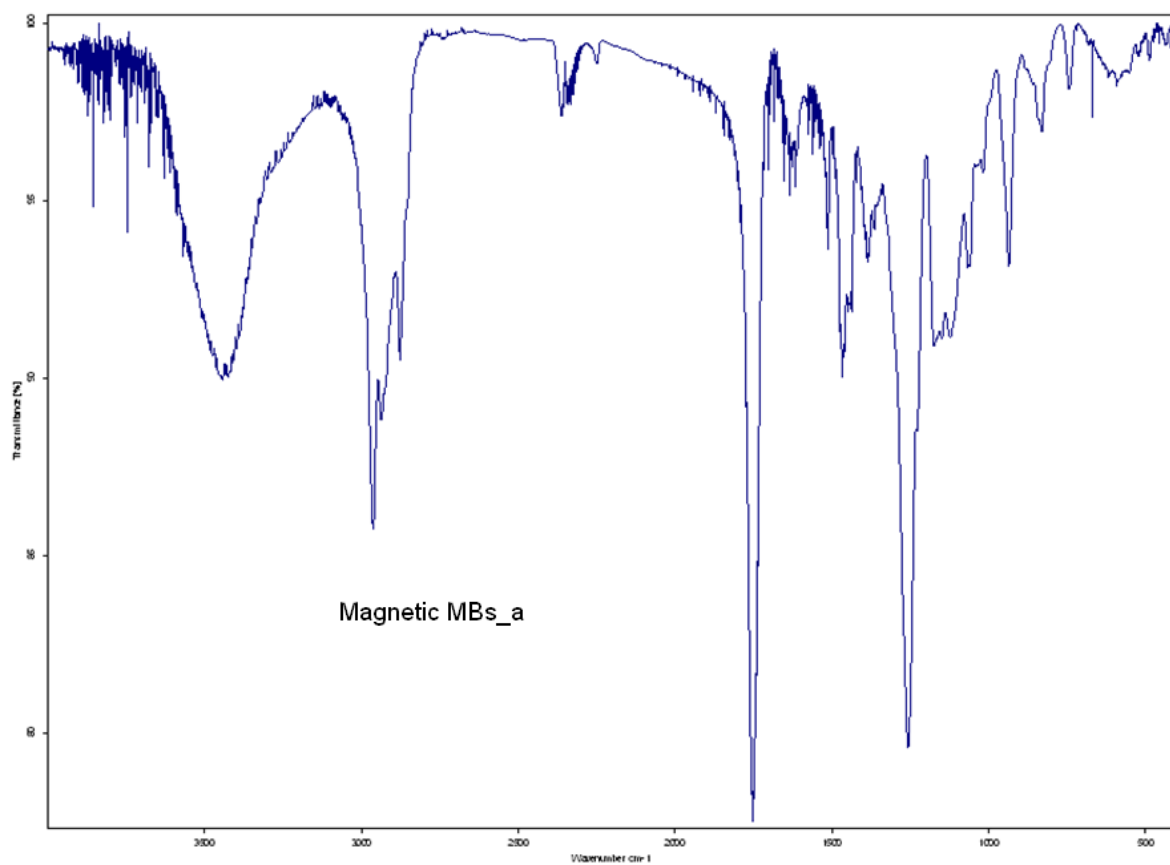


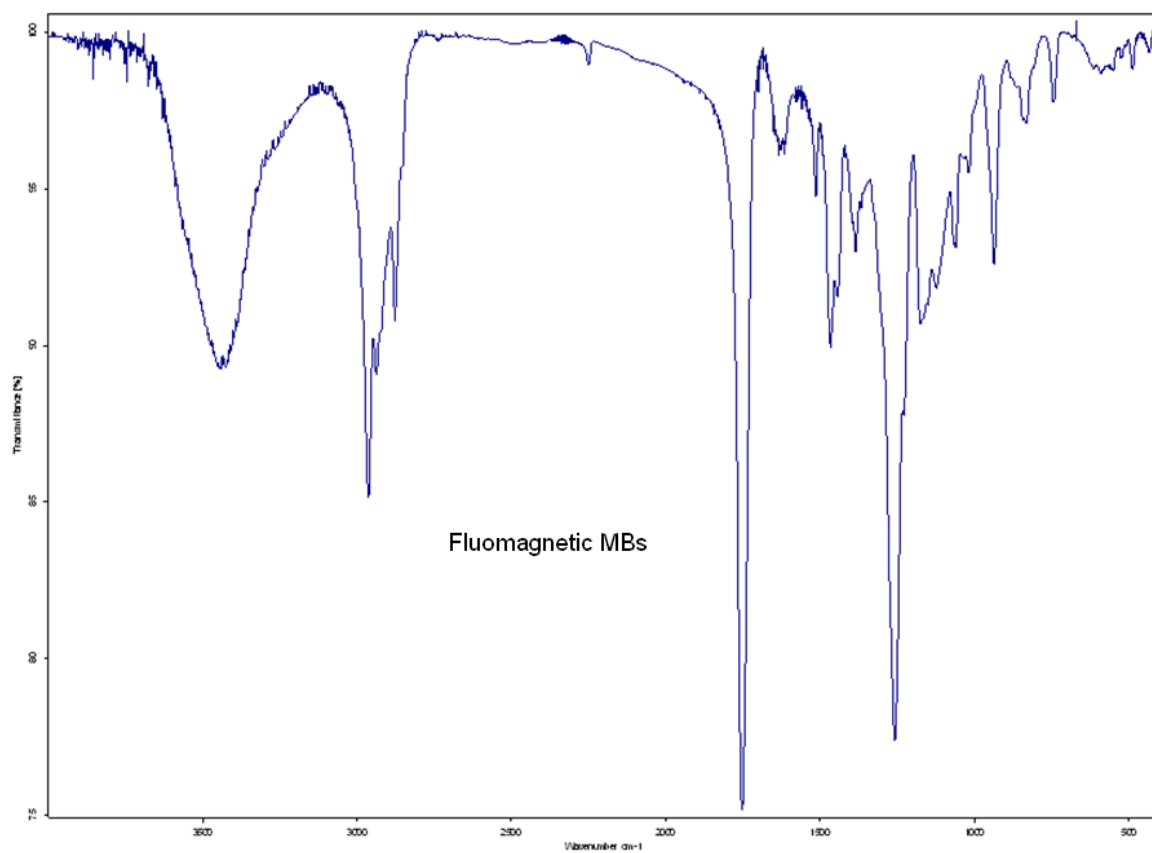
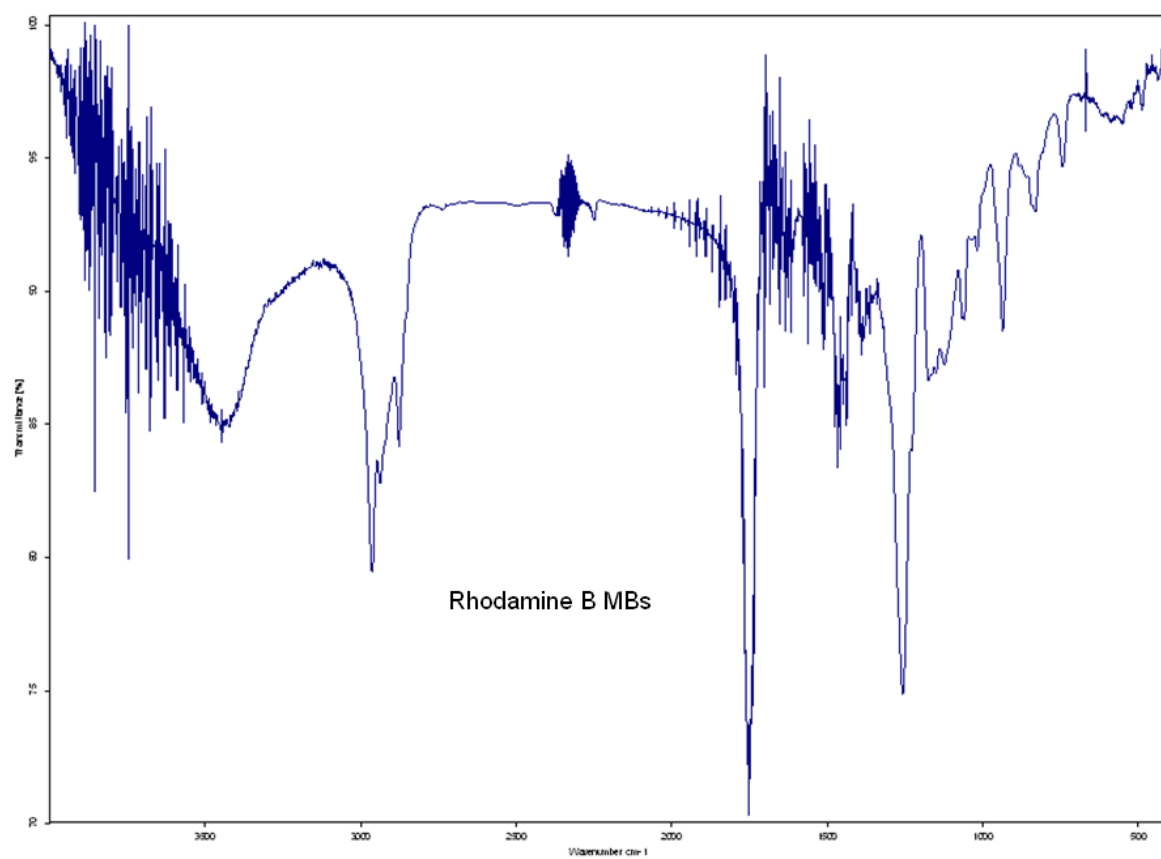
**Fig. 1S.** Centrifugation efficiency (500 rpm,  $3 \times 20$  min) to afford microbubbles with monodispersity.



(a)



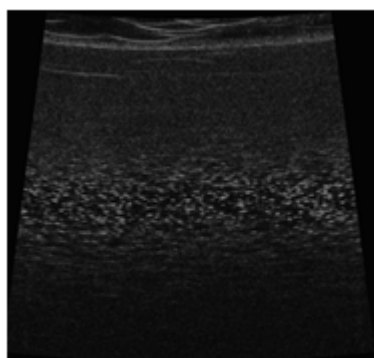




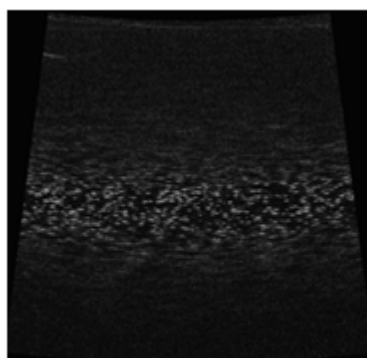
(b)

**Fig. 2S.** NMR (a) and IR (b) characterizations of synthesized microbubbles.





Pure MBs



Fluomag MBs

**Fig. 3S.** Comparison of Pure and Fluomag MBs by modality of ultrasound (US) imaging.

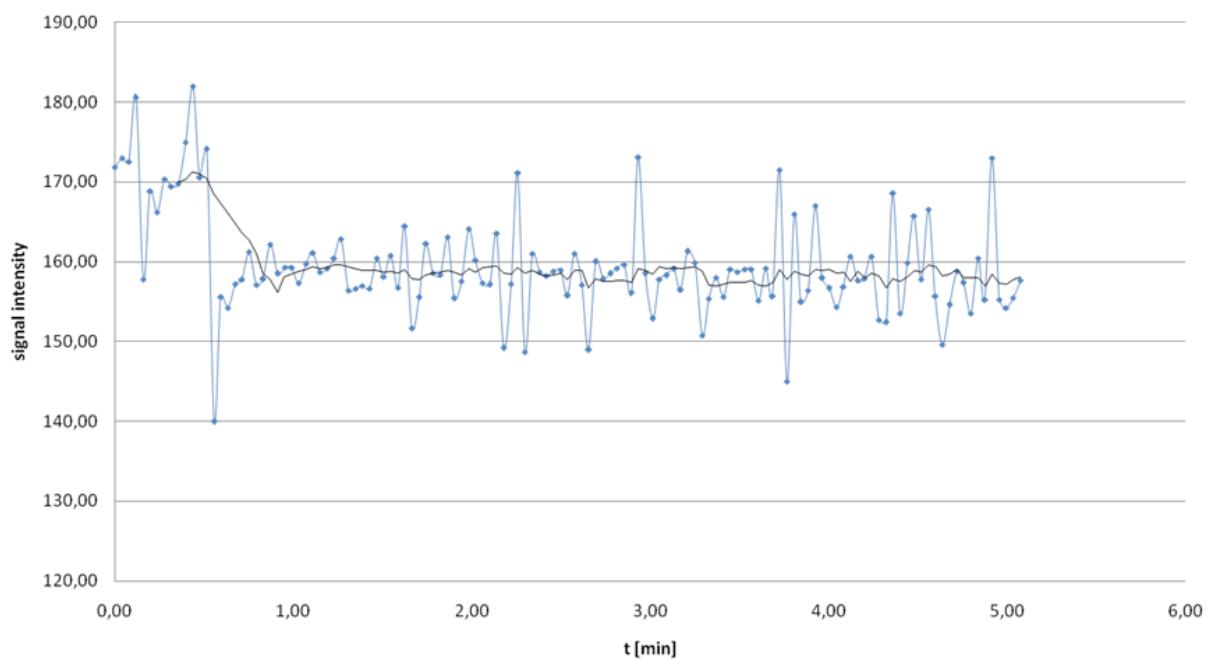


**Fig. 4S.** T2\*-weighted EPI DCE MR imaging with VEGFR2-targeting fluomagnetic microbubbles.